Computational Modeling of the Thermally Stressed State of a Partially Insulated Variable Cross-Section Rod

Zhuldyz Tashenova[1], Elmira Nurlybaeva[2], Zhanat Abdugulova[3],
Shirin Amanzholova[4], Nazira Zharaskhan[5], Aigerim Sambetova[6], Anarbay Kudaykulov[7]
Department of Information Technologies, L. N. Gumilyov Eurasian National University, Astana, Kazakhstan[1, 3, 5]
Department of Computer technologies, T.K. Zhurgenov Kazakh National Academy of Arts, Almaty, Kazakhstan[2, 6]
Department of Social and Humanitarian Disciplines, The Kurmangazy Kazakh National Conservatory, Almaty, Kazakhstan[4]
Department of IT Institute of Information and Computational Technologies, Almaty, Kazakhstan[7]

***Abstract*—The formulation of the proposed methods and algorithms facilitates a comprehensive examination of intricate non-stationary thermo-mechanical processes in rods with varying cross-sectional geometries. Furthermore, it advances the theoretical framework for analyzing the thermo-mechanical properties of rod structures utilized in the machinery industry of the Republic of Kazakhstan. The creation of these intellectual products aids in the progression of this sector and fortifies the nation's sovereignty. This article delineates methods and algorithms for investigating non-stationary thermo-mechanical processes in rods with diverse cross-sectional shapes that influence global manufacturing technologies. The scientific and practical importance of this work lies in the application potential of the developed approach for examining non-stationary thermo-mechanical characteristics of rod-like elements in various installations. The findings also enhance the scientific research direction in mechanical engineering. In conclusion, the article outlines future technological advancements, summarizes the research on non-stationary thermo-mechanical processes in rods with different cross-sectional geometries, and highlights significant economic benefits by facilitating the selection of reliable rods for specified operating conditions. This ensures the continuous and dependable operation of machinery used in mechanical engineering.**

***Keywords*—Heat flow; heat transfer; thermal expansion coefficient; thermal conductivity; modulus of elasticity**

I. Introduction

The structural components of modern gas turbine power plants, nuclear and thermal power stations, hydrogen and rocket engines, internal combustion engines, and installations for deep processing of mineral resources and oils operate within a complex force and thermal environment. The reliable operation of these systems depends on the thermo-mechanical characteristics of their load-bearing elements. Typically, these elements are considered as rods of limited length and constant cross-sectional area. In related studies, temperature distribution along the length of such rods is determined based on fundamental thermophysics laws, considering the types of heat sources acting on them. Unlike those, the current work focuses on a horizontal rod of limited length and constant cross-sectional area, fully thermally insulated on its lateral surface. A constant heat flux is applied to the left end, while the right end exchanges heat with the environment.

Using fundamental energy conservation laws, this study determines the temperature distribution along the rod, its thermal elongation, the axial compressive force generated, and the distribution of elastic, temperature, and thermoelastic deformations and stresses, as well as the displacement field. Understanding the temperature distribution along the rod is crucial for the thermal stress state in bearing components of power plants and engines.

Previous works such as [1] and [2] have explored the principles of elasticity theory and numerical methods for applied mechanics. The primary thermo-physics equations, detailed in [3], include mass, momentum, and energy conservation. Other studies, like [4], [5], and [6], have investigated contact heat transfer and the thermal stress-strain state under various conditions, using the finite element method [7]. Additionally, [8] and [9] have addressed stress-strain states in rigid plastic pipes and nonlinear finite element modeling, while [10] and [11] discussed adiabatic shear bands and nonlinear continuum mechanics.

In [12], the temperature distribution within nuclear fuel rods was analyzed, highlighting the importance of maintaining fuel integrity. Research in [13], [14], and [15] derived computational relationships for thermal forces in rectangular cross-section rods. Other studies, such as [16], examined the thermal behavior of bars during hot rolling. The finite element method was also employed in [17] and [18] to model temperature fields in Terfenol-D rods, while [19] investigated unstable temperature distributions in cylindrical rods subjected to laser heat sources.

This body of work supports the development of a mathematical model for the thermomechanical state of a variable cross-section rod, considering local temperature, thermal insulation, and heat exchange. Scientific works [20]-[26] provide analytical solutions for compressive extensions and force distributions in thermally insulating rods, based on energy conservation principles. This paper diverges by using quadratic spline functions to address a specific practical

problem, offering a novel approach to understanding the thermomechanical behavior of such rods.

II. Materials and Methods

Let's consider a rod of finite length clamped at both ends, whose cross-section varies along its length and is circular. In this case, the radius of the cross-section depends linearly on the coordinates. The radius of the left end is denoted by r_0, the radius of the right end by r_L, and the length of the rod by L. Thus, the radius as a function of the coordinate x is given by the following expression [20]:

$$r = \frac{r_L - r_0}{L} \cdot x + r_0 \quad (1)$$

where x is the coordinate along the length of the rod, ranging from 0 (left end) to L (right end) (Fig. 1).

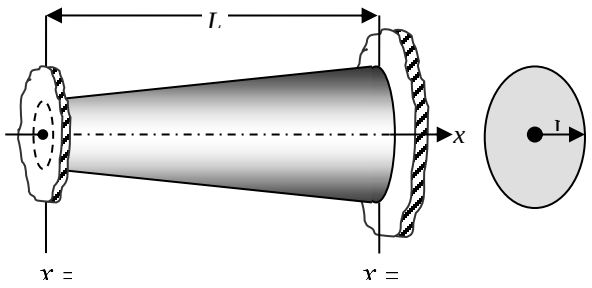

Fig. 1. Calculation diagram of the problem.

The temperature is fixed at the left clamped end as $T(x = 0) = T_1$, and at the right end as $T(x = L) = T_{2n+1}$. The lateral surfaces of the sections $(0 \le x \le x_1)$, $(x_2 \le x \le x_3)$ and $(x_4 \le x \le x_L)$ are thermally insulated. In the section $(x_1 \le x \le x_2)$ heat exchange with the environment occurs through the lateral surface area, with a heat transfer coefficient h, and an ambient temperature T_{co}. Additionally, a heat flux of constant intensity q is applied to the lateral surface area in the section $(x_3 \le x \le x_4)$ The objective is to numerically investigate the influence of the temperature value $T_0 \in [(-150\ C) \div (+150\ C)]$ on the system.[21].

On the temperature distribution field $(T = T(x))$, elastic displacement $(u = u(x))$, as well as components of deformation $(\varepsilon_x = \varepsilon_x(x);\ \varepsilon_T = \varepsilon_T(x);\ \varepsilon = \varepsilon(x))$ and voltage $(\sigma_x = \sigma_x(x);\ \sigma_T = \sigma_T(x);\ \sigma = \sigma(x))$. To develop a mathematical model of the temperature distribution along the length of the considered partially thermally insulated rod of finite length, the rod is discretized using quadratic elements with three nodes. The total number of elements is denoted by n. Consequently, the total number of nodes will be $(2n + 1)$. The discretization is performed in such a manner that the element boundaries coincide with the boundaries of the thermally insulated regions of the rod. For each element, a functional expression is derived that characterizes its total thermal energy. Specifically, for elements belonging to the thermally insulated sections of the rod, the functional I_i is given by:

$$I_i = \int_{V_i} \frac{K_{xx}}{2} \left(\frac{\partial T}{\partial x}\right)^2 \mathrm{dV}, (i = 1, 2, \ldots) \quad (2)$$

Here, K_{xx} represents the thermal conductivity coefficient along the *x*-axis, T is the temperature, and V_i is the volume of the *i-th* element. This integral expression accounts for the thermal energy stored within each element due to the temperature gradient along the rod. Where V_i- volume of the *i-th* element.

For elements located on the section of the rod where heat exchange occurs through the lateral surface, the expression for the corresponding functional takes into account both the internal thermal energy due to the temperature gradient and the heat exchange with the environment [22].

$$I_j = \int_{V_j} \frac{K_{xx}}{2} \left(\frac{\partial T}{\partial x}\right)^2 \mathrm{dV} + \int_{S_{\text{jПБП}}} \frac{h}{2} (T - T_{co})^2 \mathrm{dS}, (j = 1, 2, \ldots) \quad (3)$$

Where V_j- volume of the *j-th* element, $S_{\text{jПБП}}$- area of the lateral surface of the *j-th* element.

For elements located on a section of the rod where a heat flux of constant intensity q is supplied through the lateral surface, the functional expression that characterizes their total thermal energy includes contributions from both the internal thermal energy due to the temperature gradient and the external heat flux applied to the surface.

$$I_k = \int_{V_k} \frac{K_{xx}}{2} \left(\frac{\partial T}{\partial x}\right)^2 \mathrm{dV} + \int_{S_{\text{kПБП}}} \mathrm{qT}(x) \mathrm{dS}, (k = 1, 2, \ldots) \quad (4)$$

The general expression for the functional of total thermal energy for a partially thermally insulated rod with a variable cross-section, accounting for local temperatures, heat flux, and heat transfer, can be derived by combining the contributions from different sections of the rod. These contributions include the internal thermal energy due to the temperature gradient, heat exchange with the environment, and the applied heat flux.

$$I = \sum_{t=1}^{n} I_t \quad (5)$$

To construct a mathematical model of the temperature distribution field along the length of the rod, the functional representing the total thermal energy must be minimized with respect to the nodal temperature values. This minimization leads to a system of linear algebraic equations, which can be solved to obtain the temperature distribution

$$\frac{\partial I}{\partial T_t} = 0, (t = 2, 3, \ldots, 2n) \quad (6)$$

Because T_1 and T_{2n+1} are considered given, then the number of equations in system (6) will be equal to $(2n + 1)$.

Solving the system for different values T_1 and fixed values T_{2n+1}, h,T_{co}, as well as q, the influence of T_1 on the nature of the temperature distribution field along the length of the rod in question.[23].

After constructing the temperature distribution field along the length of the rod, the next step is to develop a mathematical model for the distribution field of elastic displacement, as well as the components of deformation (strain) and stress. This model is crucial for understanding the mechanical response of the rod to the thermal loads. To do this, the rod under study is discretized $\left(N = \frac{n}{2}\right)$ quadratic elements with three nodes. After obtaining the temperature distribution and determining the displacement field, the next step is to write the expression for the functional of the potential energy of elastic deformation for each element. This functional represents the elastic energy

stored in the rod due to the deformation caused by both mechanical and thermal effects.

$$\Pi_i = \int_{V_i} \frac{\sigma_x \varepsilon_x}{2} \mathrm{dV} - \int_{V_i} \alpha \mathrm{ET}(x) \mathrm{dV}, (i = 1, 2, ..., N) \quad (7)$$

Where V_i - volume of the *i-th* element, $u = u(x)$ - elastic displacement distribution field, $\varepsilon_x = \frac{\partial u}{\partial x}$ - distribution field of the elastic component of deformation, $\sigma_x = E\varepsilon_x = E \cdot \frac{\partial u}{\partial x}$ - distribution field of the elastic component of stress, E - elastic modulus of the rod material, α - coefficient of thermal expansion of the rod material, $T = T(x)$ - temperature distribution field determined from the solution of system (6).

For the considered rod as a whole, the expression for the potential energy of elastic deformation is as follows:

$$\Pi = \sum_{i=1}^{N} \Pi_i \quad (8)$$

To construct a mathematical model for the distribution of elastic displacement along the length of the rod, the functional of the potential energy of elastic deformation is minimized with respect to the nodal values of the elastic displacement. This minimization leads to a system of linear algebraic equations that describe the elastic displacement field.[26].

$$\frac{\partial \Pi}{\partial u_i} = 0, (i = 1, 2, ..., (2N + 1)) \quad (6)$$

Solving this system, the elastic displacement distribution field is determined $u = u(x)$ along the length of the rod in question. Based on them, the corresponding fields for the distribution of the components of deformation and stress are constructed as follows:

$$\varepsilon_x = \frac{\partial u}{\partial x}; \varepsilon_T = -\alpha T(x); \varepsilon = \varepsilon_x + \varepsilon_T \quad (10)$$

$$\sigma_x = E\varepsilon_x; \sigma_T = E\varepsilon_T; \sigma = (\sigma_x + \sigma_T) \quad (11)$$

To carry out numerical studies, we take the following as initial data:

$L = 20$ (cm), $r_0 = 1$ (cm), $r_\ell = 2$ (cm), $n = 200$, $N = \frac{n}{2} = 100$, $q = -1000$ (W/cm^2), $K_{xx} = 100$ (W/(cm $\cdot$ C)), $h = 10$ (W/(cm^2 $\cdot$ C)), $T_{co} = 40\ (C)$, $T_{401} = 150\ (C)$, and vary the value $T_1 \in [(-150\ C) \div (+150\ C)]$ in increments $(-50\ C)$.

Consider the following 7 options. In all options except value T_1, the values of all parameters are fixed.

III. Results and Discussion

A. Option-1

Consider the case when $T_1 = 100\ (C)$, i.e. previous value $T_1 = 150\ (C)$ let's reduce it by 1/3. In this case, the nodal temperature values are given in Table I. The corresponding field temperature distribution is given in Fig. 2. From them it is clear that the highest nodal temperature value will be $T_{277} = 262{,}089\ (C)$. The coordinate of this section $x = 13{,}8$ (см), that the phenomenon is caused by the supply to the closed side surface of the area1 $2 \le x \le 16$ (см) heat flux rod of constant intensity $q = -1000$ (W/cm^2). Reducing the nodal temperature values on the site $4 \le x \le 8$ (cm) the rod is due to the ongoing heat exchange with the surrounding closed side surface of this section. Therefore, the smallest nodal temperature value $T_{89} = 85{,}603\ (C)$. The coordinate of this section $x = 4{,}4$ (см).

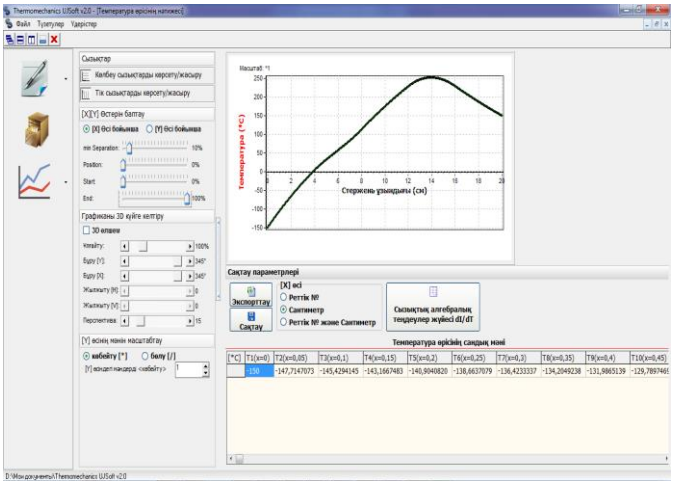

Fig. 2. Field temperature distribution at different values $T(x = 0) = T_1$.

TABLE I. Nodal Temperature Values

Nodal points	$T\ (^\circ C)$	Nodal points	$T\ (^\circ C)$	Nodal points	$T\ (^\circ C)$	Nodal points	$T\ (^\circ C)$
1	100,00	101	87,031	201	192,399	301	253,884
2	99,793	102	87,267	202	193,712	302	253,199
3	99,586	103	87,522	203	195,025	303	252,485
...	...	...	...	...	...	...	...
10	98,170	110	89,802	210	204,078	310	246,763
20	96,229	120	94,601	220	216,659	320	236,416
30	94,378	130	101,289	230	228,839	330	224,721
40	92,611	140	110,009	240	240,639	340	213,328
50	90,923	150	120,969	250	250,826	350	202,240
60	89,309	160	134,441	260	257,685	360	191,444
70	87,764	170	149,334	270	261,349	370	180,928
80	86,283	180	163,729	280	261,960	380	170,683
90	85,622	190	177,635	290	259,650	390	160,697
100	86,812	200	191,078	300	254,545	400	150,961
						401	150,000

Table II presents the nodal displacement values. The corresponding field distribution of displacements along the length of the considered rod of variable cross-section is given in Fig. 3. From these it is clear that all sections of the rod under study move against the direction of the Ox axis. In this case, the section of the rod with the coordinate $x = 8{,}8$ (cm) moves more than others i.e. $u_{89} = -0{,}0142153$ (cm).

Fig. 4 their corresponding distribution field along the length of the rod under consideration is given. From them it is clear that on the site $0 \le x \le 8{,}75$ (cm) of the rod, the behavior of the elastic component of the deformations will be compressive, and then tensile. At the same time, the greatest compressive ε_x corresponds near the left pinched end. Highest tensile value $\varepsilon_x = 0{,}0018518$ which corresponds to the section coordinate $x = 14{,}45$ (cm). Corresponding field distribution ε_T along the length of the rod in question is given by Fig. 6. It

should be noted that along the entire length of the rod under study ε_T has a compressive character. Its greatest value corresponds to the section with coordinate $x = 13{,}85$ (cm). Here $\varepsilon_T = -0{,}0032759$. The corresponding field distribution is given in Fig. 6. From these it is clear that starting from the left pinched end of the rodεfalls monotonously. But along the entire length of the rod it has a compressive character. Its greatest value corresponds to the left pinched end of the rod. Near the left end its value is equal to $\varepsilon = -0{,}0041062$.

TABLE II. NODAL DISPLACEMENT VALUES

Nodal points	u $(см)$	Nodal points	u $(см)$	Nodal points	u $(см)$	Nodal points	u $(см)$
1	0,000000	51	-0,010882	101	-0,0138770	151	-0,006699
2	-0,000285	52	-0,011036	102	-0,0138180	152	-0,006517
3	-0,000572	53	-0,011190	103	-0,0137557	153	-0,006337
…	…	…	…	…	…	…	…
10	-0,002465	60	-0,012174	110	-0,0131918	160	-0,005114
20	-0,004907	70	-0,013294	120	-0,0120301	170	-0,003543
30	-0,007077	80	-0,014002	130	-0,0104933	180	-0,002187
40	-0,009009	90	-0,014212	140	-0,0087232	190	-0,001037
50	-0,010723	100	-0,013930	150	-0,0068811	200	-0,000084
						201	0,000000

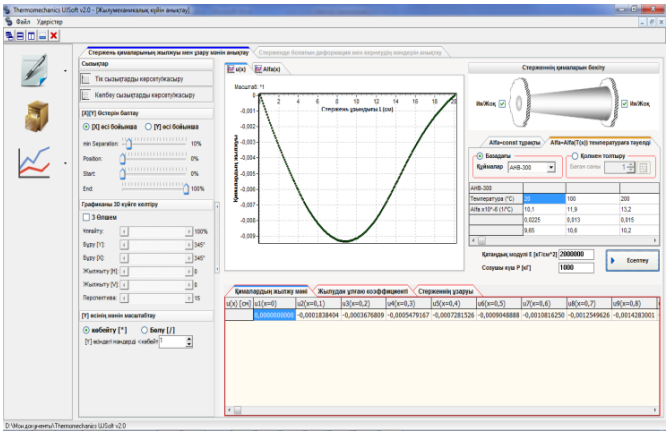

Fig. 3. Distribution field displacement at different values $T(x = 0) = T_1$.

The field distribution of these stress components along the length of the rod is given in Fig. 5. From these materials it is clear that the elastic component of the stress σ_x location on $0 \le x \le 8{,}75$ (cm) the rod behaves compressively, and then has a tensile character. Temperature component voltage σ_T along its entire length it has a compressive character. Its greatest value $\sigma_T = -6551{,}887$ (kG/cm^2). This corresponds to the section whose coordinate $x = 13{,}85$ (cm). Thermoelastic stress component $\sigma = \sigma_x + \sigma_T$ along its entire length it has a compressive character. Its highest value corresponds to the left pinched end of the rod, i.e. $\sigma = -8212{,}409$ kG/cm^2). Starting from left to right, it monotonically decreases and at the right pinched end it has the smallest value $\sigma = -2084{,}123$ (kG/cm^2). In this case, the magnitude of the compressive force $R_2 = \sigma_n(x = 0{,}05) \cdot F_n = -25929{,}2052$ (kG). Naturally, this is less than in the case$T_1 = 150$ (C) by 5.4%.

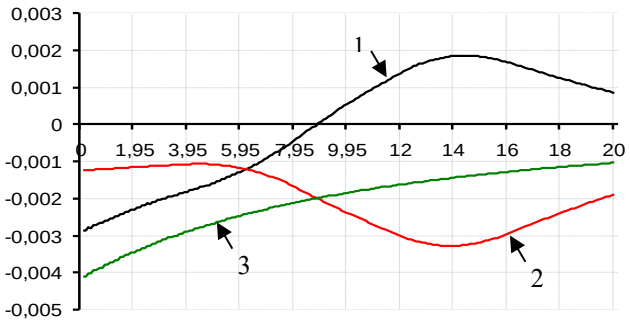

$1 - \varepsilon_x; 2 - \varepsilon_T; 3 - \varepsilon = \varepsilon_x + \varepsilon_T$

Fig. 4. Field distribution of strain components at $T(x = 0) = T_1 = 100$ (C).

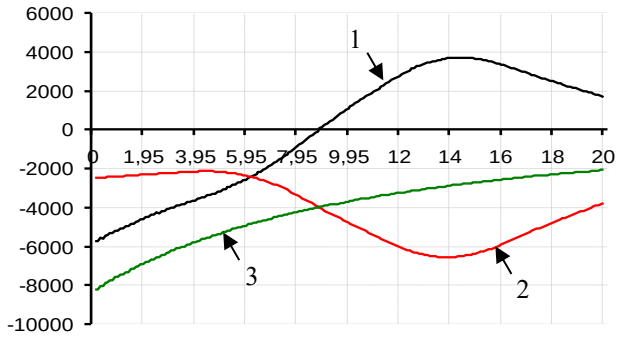

$1 - \sigma_x; 2 - \sigma_T; 3 - \sigma = \sigma_x + \sigma_T$

Fig. 5. Field distribution of voltage components at $T(x = 0) = T_1 = 100$ (C).

Now consider the next option.

B. Option-2

Compared to option 1, in this option the value of the set temperature T_1 l let's reduce it by three times, i.e. let's accept $T_1 = 50\ (C)$. In this case, the nodal temperature values are presented in Table III. The temperature distribution corresponding to the field along the length of the rod under study is shown in Fig. 2. In this case, the highest temperature value will be $T_{278} = 260{,}034\ (C)$. This temperature value corresponds to the section of the rod whose coordinate $x =$ 13,85 (cm). Naturally, this is due to the supplied heat flow of constant intensity and power$q = -1000$ (W/cm^2)on the side surface areas $12 \le x \le 16$ (cm) rod.

The distribution field of the displacement field is given in Fig. 3. From these data it is clear that all sections of the rod under study move against the direction of the Ox axis. When the section moves the most, the coordinate of which $x =$ 8,7 (cm). This section moves against the direction of the Ox axis by $u_{88} = -0{,}0148657$ (cm).

TABLE III. NODAL TEMPERATURE VALUES ($T_1 = 50\ (^\circ C)$)

Nodal points	$T\ (^\circ C)$	Nodal points	$T\ (^\circ C)$	Nodal points	$T\ (^\circ C)$	Nodal points	$T\ (^\circ C)$
1	50,000	101	75,942	201	188,655	301	252,280
2	50,292	102	76,389	202	189,993	302	251,613
3	50,583	103	76,850	203	191,330	303	250,917
...	...	...	...	...	...	...	...
10	52,578	110	80,437	210	200,555	310	245,321
20	55,314	120	86,740	220	213,374	320	235,151
30	57,922	130	94,577	230	225,785	330	223,627
40	60,411	140	104,153	240	237,808	340	212,401
50	62,790	150	115,724	250	248,213	350	201,475
60	65,064	160	129,596	260	255,281	360	190,837
70	67,242	170	144,773	270	259,149	370	180,475
80	69,329	180	159,441	280	259,958	380	170,380
90	71,831	190	173,611	290	257,840	390	160,540
100	75,506	200	187,308	300	252,922	400	150,947

The field-corresponding distribution of these components along the length of the rod in question is shown in Fig. 6.

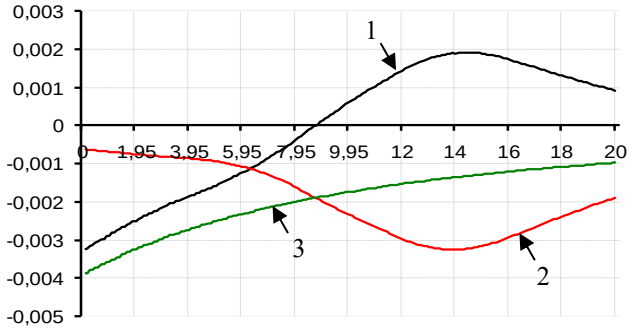

$1 - \varepsilon_x;\ 2 - \varepsilon_T;\ 3 - \varepsilon = \varepsilon_x + \varepsilon_T$

Fig. 6. Field distribution of strain components at$T(x = 0) = T_1 = 50\ (C)$.

From these data it is clear that the behavior of the elastic deformation component in the area $0 \le x \le 8{,}65$ (cm)the rod will be compressive, and then tensile. In this case, the largest compressive elastic component of deformations ε_x falls close to the left clamped end of the test rod of variable cross-section, $\varepsilon_x = -0{,}0032431$. Greatest tensile ε_x corresponds to the section with coordinate $x = 14{,}45$ (cm). In this section the value ε_x will $\varepsilon_x = 0{,}0019087$. Behavior of the temperature component ε_T along the entire length of the rod will be compressive. At the same time, the greatest compressive ε_T corresponds to the section with coordinate $x = 13{,}85\ (cm)$. In this section $\varepsilon_T = -0{,}0032504$.

Unlike ε_x and ε_T field distribution of the thermoelastic component of deformations $\varepsilon = \varepsilon_x + \varepsilon_T$ will be described by a smooth curve. Along the entire length of the rod it has a compressive character. Moreover, its greatest value $\varepsilon = -0{,}0038718$ corresponds closer to the left pinched one, and the smallest $\varepsilon = -0{,}0009826$ closer to the right end.

Nodal values of all three stress components (σ_x,σ_T and $\sigma = \sigma_x + \sigma_T$) their field distributions along the length of the rod of variable cross-section under study are shown in Fig. 7.

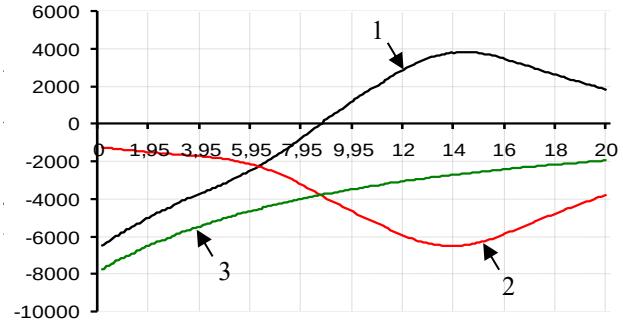

$1 - \sigma_x;\ 2 - \sigma_T;\ 3 - \sigma = \sigma_x + \sigma_T$

Fig. 7. Field distribution of voltage components at $T(x = 0) = T_1 =$ $50\ (C)$.

From these results it is clear that the values of these stress components are directly proportional to the values of the corresponding strains. In addition, in this case the value of the compressive force will be $R_3 = \sigma_n(x = 0{,}05) \cdot F_n = -24448{,}9304$ (kG) . This value is 10.8% less than the compressive force that occurs when $T_1 = 150\ (C)$.

C. Option-3

Now consider the fourth option, when $T_1 = 0\ (C)$. The corresponding field temperature distribution along the length of the test rod of variable cross-section is given in Fig. 2.

The corresponding displacement distribution fields along the length of the rod under study are shown in Fig. 3. It should be noted here that, except for the pinched ends, all sections of the rod move against the direction of the *Ox* axis. At the same time, in this direction the section whose coordinate moves more $x = 8{,}6$ (cm). The displacement value of this section $u_{87} = -0{,}0155244$ (cm).

The corresponding field distribution along the length of the rod under study is shown in Fig. 8.

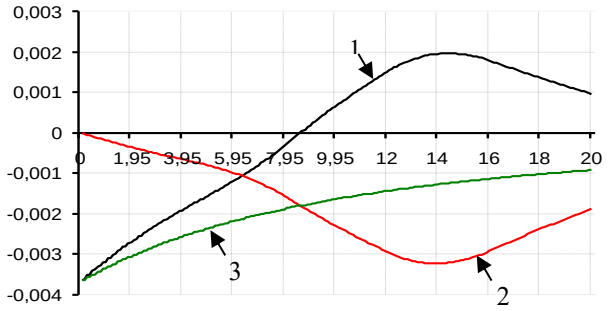

$1-\varepsilon_x; 2-\varepsilon_T; 3-\varepsilon=\varepsilon_x+\varepsilon_T$

Fig. 8. Field distribution of strain components at $T(x=0)=T_1=0\ (C)$.

From these results it is clear that in the area $0 \le x \le$ 8,55 (cm)behavior of the rod elastic component of deformation ε_x will be compressive, and then tensile. In this case, the greatest compressive ε_x corresponds near the left pinched end. The highest value of the compressive elastic component of deformation $\varepsilon_x=-0{,}0036275$, and tensile $\varepsilon_x=0{,}0019657$ and it corresponds to the section with coordinate $x=$ 14,45 (cm) rod. Behavior of the temperature component of deformation ε_T along the entire length of the rod will be compressive. In this case, its lowest value corresponds near the left pinched end, and its highest value $\varepsilon_T=-0{,}0032249$ corresponds to the section with coordinate $x=13{,}85$ (cm) rod. As can be seen from Fig. 8 field distribution of the thermoelastic component of deformation $\varepsilon=\varepsilon_x+\varepsilon_T$ is described by a smooth monotonically increasing curve. At the same time, behaviorεalong the entire length of the rod under study will be compressive. Its greatest value occurs near the pinched left end of the rod and will be equal to $\varepsilon=-0{,}0036374$. Its smallest value corresponds closer to the right pinched end of the rod under study.

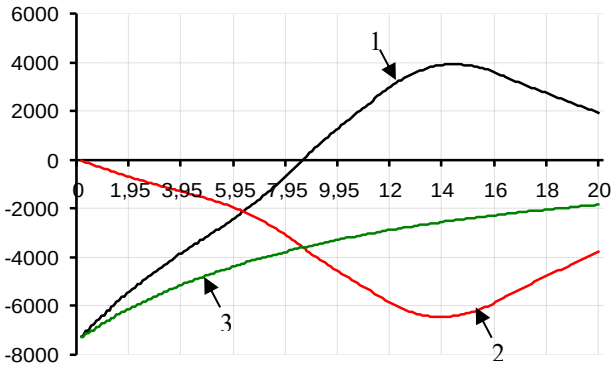

$1-\sigma_x; 2-\sigma_T; 3-\sigma=\sigma_x+\sigma_T$

Fig. 9. Field distribution of voltage components at $T(x=0)=T_1=0\ (C)$.

The field distribution of these voltage components is given in Fig. 9. Naturally different behavior matches behavior ε_x,ε_T and $\varepsilon=\varepsilon_x+\varepsilon_T$. The values of these stress components will be proportional to the corresponding strain components. In this case, the compressive force values R_4 will be equal $R_4=\sigma_n(x=0{,}05)\cdot F_n=-22968{,}6555$ (kG). This is less than R_1(in the case when $T_1=150\ (C)$) by 16.2%.

Now let's look at the fifth option.

D. Option-4

In this version we will accept $T_1=-50\ (C)$. The corresponding temperature distribution field along the length of the rod of variable cross-section under study is shown in Fig. 2. In this case, the maximum nodal temperature values $T_{\max}=T_{279}=255{,}968\ (C)$ and it corresponds to the cross section of the rod in question whose coordinate $x=13{,}9$ (cm).

The corresponding distribution field on Fig. 3. In this case, all sections of the rod move against the direction of the *Ox* axis. In this direction the greatest movement of the section of the rod whose coordinate is $x=8{,}4$ (cm). The displacement value of this section $u_{\max}=u_{85}=-0{,}0161891$ (cm).

The field-corresponding distributions of these strain components are shown in Fig. 10.

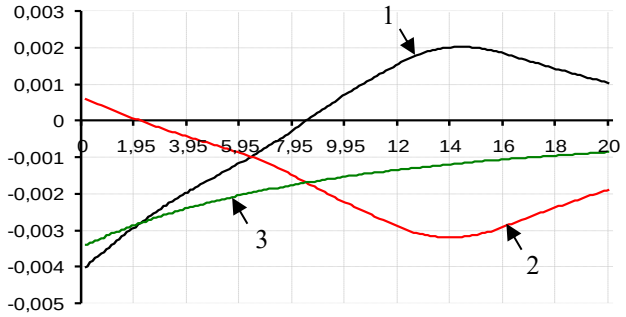

$1-\varepsilon_x; 2-\varepsilon_T; 3-\varepsilon=\varepsilon_x+\varepsilon_T$

Fig. 10. Field distribution of strain components at$T(x=0)=T_1=-50\ (C)$.

From these results it is clear that the behavior of the elastic component of deformations ε_x l ocation on $0 \le x \le$ 8,35 (cm) of the rod under study will be compressive, and then tensile. Highest compressive value $\varepsilon_x=-0{,}0040118$ and it corresponds near the left pinched end of the rod. In this case, the largest tensile value of the strain component $\varepsilon_x=$ 0,0020226 and it corresponds to the section with coordinate $x=14{,}45$ (cm) rod. Unlike previous options, the behavior of the temperature component of deformations ε_T will be alternating. Location on $0 \le x \le$ 2,05 (cm) core behavior ε_T will be tensile, and then it behaves compressively. In this case, the greatest tensile value ε_T observed near the left pinched end and it is equal $\varepsilon_T=$ 0,0006089. Location on $2{,}15 \le x \le L=20$ (cm) rod behavior ε_T will be compressive. Maximum compressive temperature component of deformation ε_T will be equal $\varepsilon_T=-0{,}0031994$ and it occurs in the section of the rod whose coordinate is $x=13{,}95$ (cm). Behavior of the thermoelastic component of deformations $\varepsilon=\varepsilon_x+\varepsilon_T$ along the entire length of the rod will have a compressive character. It should be noted that the values ε starting from the left pinched end, it monotonically decreases along the length of the studied rod of

variable cross-section. The highest value $\varepsilon = -0{,}0034029$ which corresponds to the left pinched end of the rod. Near the right pinched end of the test rod, the value ε will be the smallest and will be equal $\varepsilon = -0{,}0008636$.

The distribution of these stress components corresponding to them along the length of the rod of variable cross-section under study is given in Fig. 11.

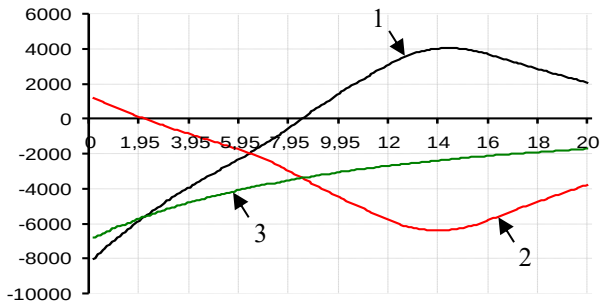

$1-\sigma_x;\ 2-\sigma_T;\ 3-\sigma=\sigma_x+\sigma_T$

Fig. 11. Field distribution of voltage components at $T(x=0)=T_1=-50\ (C)$.

Location on $0 \le x \le 8{,}35$ (cm) behavior of the elastic component of stress of the rod under study σ_x will be compressive. In this case, the highest compressive stress σ_x observed near the left pinched end and will $\sigma_x = -8023{,}682\ (\text{kG/cm}^2)$. On another part of the rod $8{,}45 \le x \le L = 20$ (cm)behavior σ_x will be stretchy. Moreover, its greatest value $\sigma_x = 4045{,}210\ (\text{kG/cm}^2)$ observed near the section whose coordinate $x = 14{,}45$ (cm). Unlike σ_x behavior of the temperature component of voltage σ_T location on $0 \le x \le 2{,}05$ (cm) the rod under study will be tensile. More over, its greatest value $\sigma_T = 1217{,}790\ (\text{kG/cm}^2)$observed near the left pinched end. On the rest of the behavior rod σ_T will be compressive. The highest value of compressive stress $\sigma_T = -6398{,}852\ (\text{kG/cm}^2)$ observed in the section whose coordinate $x = 13{,}95$ (cm) . Behavior of the thermoelastic stress component $\sigma = \sigma_x + \sigma_T$ along the entire length of the rod under study will have a compressive character. Its greatest value $\sigma(x = 0{,}05) = -6805{,}893\ (\text{kG/cm}^2)$ observed at the left pinched end of the rod. As the length of the rod increasesσits value decreases monotonically and near the right pinched end $\sigma(x = 19{,}95) = -1727{,}199\ (\text{kG/cm}^2)$, i.e.$\frac{\sigma(x=0{,}05)}{\sigma(x=19{,}95)} = 3{,}94$ times. From the obtained values $\sigma = \sigma_x + \sigma_T$ let's calculate the value of the compressive $R_5 = \sigma_n(x = 0{,}05) \cdot F_n = -21488{,}3838$ (kG).

Now consider the next sixth option.

E. Option-5

In this option, we assume that the given value is $T_1 = -100\ (C)$. In this case, the field temperature distribution along the length of the considered rod of variable cross-section is shown in Fig. 2. From Fig. 2 it is clear that the highest temperature value, $T_{280} = 253{,}952\ (C)$and it corresponds to the section of the rod whose coordinate $x = 13{,}95$ (cm).

The corresponding field of elastic displacement of sections of the rod is shown in Fig. 3. From Fig. 3 it can be seen that all sections of the rod under study move against the direction of the *Ox* axis. Moreover, in this direction the greatest displacement belongs to the section with the coordinate $x = 8{,}3$ (cm). The displacement value of this section will be $u_{84} = -0{,}0168614$ (cm).

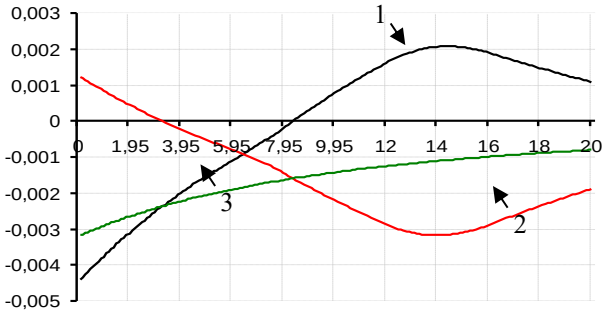

$1-\varepsilon_x;\ 2-\varepsilon_T;\ 3-\varepsilon=\varepsilon_x+\varepsilon_T$

Fig. 12. Field distribution of strain components at $T(x=0)=T_1=-100\ (C)$.

The field-corresponding displacement of these deformation components along the length of the rod under study is shown in Fig. 12. From these tables and the figure it is clear that the behavior of the elastic component of deformations along the length of the rod under study will be alternating in sign. For example, on the site $0 \le x \le 8{,}25$ (cm) rod character ε_x will be compressive, and then it has a tensile character. Maximum compressive elastic deformation $\varepsilon_x = -0{,}0043962$ observed near the left pinched end where the temperature is set $T_1 = -100\ (C)$. In this case, the maximum tensile elastic deformation $\varepsilon_x = 0{,}0020795$ corresponds to the section $x = 14{,}45$ (cm). On the contrary, the behavior of the temperature component of deformation ε_T in the initial section of the rod under study will have a tensile character, and then a compressive character. The highest value of the tensile temperature component of deformation $\varepsilon_T = 0{,}0012277$ corresponds near the left pinched end of the rod under study. At that time, the highest value of the compressive temperature component of deformation ε_T will $\varepsilon_T = -0{,}0031744$ which belongs to the section whose coordinate $x = 13{,}95$ (cm)the rod under study. In Fig. 12, it is clear that the behavior of the thermoelastic component of deformations $\varepsilon = \varepsilon_x + \varepsilon_T$ along the entire length of the rod under study will be compressive. In this case, from the left to the right end of the rod it will decrease monotonically. Highest value $\varepsilon = -0{,}0031685$ corresponds to the section near the left pinched end of the rod.

The distribution of these voltage components corresponding to the field is given in Fig. 13. The behavior of these stress components will correspond to the behavior of similar strain components. In this case, the value of the compressive force$R_6 = \sigma_n(x = 0{,}05) \cdot F_n = -20008{,}1089\ (kG)$.

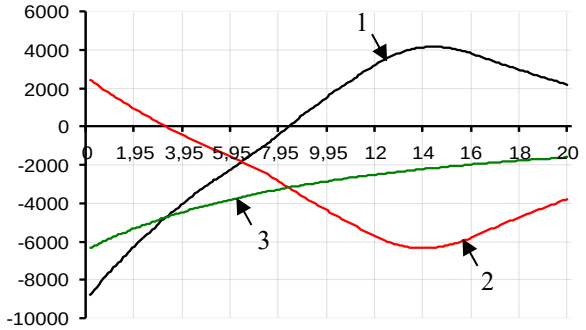

$1-\sigma_x; 2-\sigma_T; 3-\sigma=\sigma_x+\sigma_T$

Fig. 13. Field distribution of voltage components at $T(x=0)=T_1=-100\ (C)$.

Finally, let's look at the last option.

F. Option-6

In this option the value T_1 let's accept $T_1=-150\ (C)$. Field temperature distribution along the length of the test rod of variable cross-section in the case $T_1=-150\ (C)$ shown in Fig. 2. In this case, the highest temperature value $T_{280}=251{,}950\ (C)$ corresponds to the section whose coordinate $x=13{,}95\ (cm)$.

The corresponding displacement field is shown in Fig. 3. From these results it is clear that all sections of the rod except the clamped ones move against the direction of the *Ox* axis. In this case, the greatest movement $u_{83}=-0{,}0175417$ (cm) which corresponds to the section coordinate $x=8{,}2$ (cm).

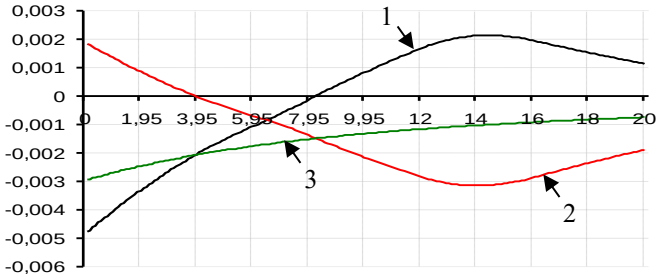

$1-\varepsilon_x; 2-\varepsilon_T; 3-\varepsilon=\varepsilon_x+\varepsilon_T$

Fig. 14. Field distribution of strain components at $T(x=0)=T_1=-150\ (C)$.

The field-corresponding distributions of these strain components are shown in Fig. 14. From Fig. 14 it is clear that the behavior of the elastic component of deformations ε_x location on $0\le x\le 8{,}15$ (cm) will be compressive, and then tensile. In this case, the greatest value of the compressive force ε_x observed near the left pinched end of the rod and will $\varepsilon_x=-0{,}0047805$. The largest value of the tensile component of deformation $\varepsilon_x=0{,}0021365$ corresponds to the section $x=14{,}45$ (cm). From Fig. 15 it is clear that the behavior of the temperature components of deformations ε_T at the initial section $0\le x\le 3{,}85$ (cm) the rod will be tensile, and then compressive. In this case, the greatest value is tensile $\varepsilon_T=0{,}0018464$ which is observed near the left pinched end of the rod. The highest compressive value $\varepsilon_T=-0{,}0031494$ which corresponds to the section whose coordinate $x=13{,}95$ (cm). From the results given Fig. 14 it is clear that the behavior of the thermoelastic component of deformations $\varepsilon=\varepsilon_x+\varepsilon_T$ along the entire length of the rod will be compressive. Moreover, as x increases, its value decreases monotonically. Highest value ε observed near the left pinched end of the rod and will be equal to $\varepsilon=-0{,}0029341$.

Table IV presents the values of the stress components σ_x, σ_T, $\sigma=\sigma_x+\sigma_T$ in the cross-sections of the studied rod. The field-corresponding distribution of these components along the length of the test rod of variable cross-section is shown in Fig. 15.

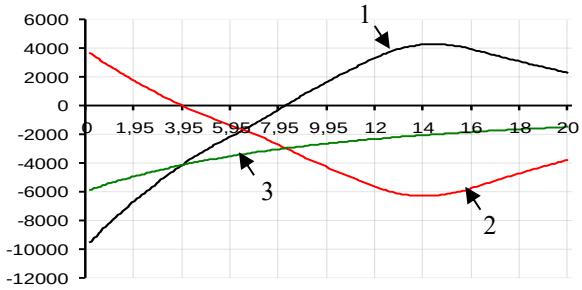

$1-\sigma_x; 2-\sigma_T; 3-\sigma=\sigma_x+\sigma_T$

Fig. 15. Field distribution of voltage components at $T(x=0)=T_1=-150\ (C)$.

TABLE IV. NODAL VALUES OF σ_x, σ_T, $\sigma=\sigma_x+\sigma_T$ AT $T_1=-150\ (^{\circ}C)$

Nodal points	Nodal points σ_x	Nodal points σ_T	Nodal points $\sigma=\sigma_x+\sigma_T$
1	-9561,083	3692,868	-5868,216
2	-9447,384	3579,169	-5868,216
3	-9219,750	3466,593	-5753,157
...	...	...	...
10	-8136,232	2708,653	-5427,579
50	-3066,817	-757,061	-3823,878
100	1653,829	-4305,735	-2651,906
150	4214,083	-6160,725	-1946,642
200	2283,025	-3772,275	-1489,250

It should be noted here that the behavior of these stress components will be like the corresponding strain components. Naturally, the value of the stress components will be proportional to the values of the corresponding strain components. In this case, the corresponding value of the compressive force $R_7=\sigma_n(x=0{,}05)\cdot F_n=-18527{,}8372$ (kG).

By analyzing the seven options considered, you can build a comparative Table I. From this table it can be seen that with

decreasing value T_1 the magnitude of the resulting compressive force R decreases. For large negative values T_1 the magnitude of the compressive force is noticeably reduced. Thus, setting the values T_1 it is possible to control the magnitude of the compressive force R arising from the distribution of the temperature field in such a way that this rod element of the variable cross-section of the structure does not collapse. We will also build Fig. 16, where a curve is given that characterizes the relationship between the resulting compressive force R and the values of the given temperature $T(x = 0)$ on the left pinched end. It should be noted here that the radius of the left end of the rod is two times smaller than the right one.

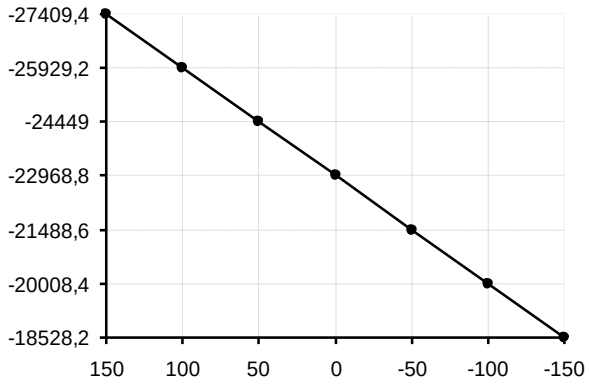

Fig. 16. Dependency between$T(x = 0)$and R.

TABLE V. INFLUENCE VALUE $T(x = 0) = T_1$BY THE MAGNITUDE OF THE RESULTING COMPRESSIVE FORCE R

No. p/p	T_1 (C)	T_{max} (C)	Coord. sections (cm)	u_{max} (cm)	Coord. section (cm)
1	150	264.153	$x = 13,75$	-0.0135704	$x = 8,9$
2	100	262,089	$x = 13,80$	-0.0142153	$x = 8,8$
3	50	260,034	$x = 13,85$	-0.0148657	$x = 8,7$
4	0	257,993	$x = 13,85$	-0.0155244	$x = 8,6$
5	-50	255,968	$x = 13,90$	-0.0161891	$x = 8,4$
6	-100	253,952	$x = 13,95$	-0.0168614	$x = 8,3$
7	-150	251,950	$x = 13,95$	-0.0175417	$x = 8,2$

IV. CONCLUSION

As a result, the following tasks were completed:

1) Algorithms have been compiled for studying local heat flows and heat transfer problems transmitted in the fields of temperature, displacement, deformation and stress on a variable rod with a cross-sectional area of finite length;

2) Algorithms and methods have been created for determining the thermal field of the side surface of an insulated column under the influence of heat flow and heat transfer.

The scientific and practical significance of the work lies in the possibility of using the developed approach to study the non-stationary thermophysical characteristics of plant elements having the shape of a rod with different cross-sectional configurations. The results also contribute to the development of research areas in mechanical engineering. The use of developed methods and algorithms for studying non-stationary thermophysical processes in rods with different transverse shapes provides significant savings, as they allow one to select a reliable rod for given operating conditions. This makes it possible to ensure continuous and reliable operation of installations used in mechanical engineering.

In the Republic of Kazakhstan, similar developments and research are practically absent.

The development of the proposed methods and algorithms makes it possible to study in detail complex non-stationary thermophysical processes in rods with different cross-sectional shapes. In addition, they make it possible to theoretically develop an appropriate methodology for studying the thermophysical characteristics of rod structures used in the engineering industry of the Republic of Kazakhstan. The development of such smart products contributes to the development of this industry and strengthens the country's sovereignty.

REFERENCES

[1] Timoshenko, S., Goodier. J. N. (1951). Theory of Elasticity. New York. Available at: http://parastesh.usc.ac.ir/files/1538886893033.pdf.

[2] Shorr, B. F. (2015). Thermoelasticity. Thermal Integrity in Mechanics and Engineering, 33–56. https://doi.org/10.1007/978-3- 662-46968-2_2.

[3] Banerjee, B. (2006). Basic Thermoelasticity. doi: http://dx.doi.org/10.13140/RG.2.1.1144.2005.

[4] Saoud, S. (2009). Etude et Analyse Mathematique des Problems Non Lineaires Modelisant les Etats Thermiques d'un Superconducteur: Generalisation au Cas Tridimensionnel.

[5] Griffith, G., Tucker, S., Milsom, J., Stone, G. (2000). Problems with modern air-cooled generator stator winding insulation. IEEE Electrical Insulation Magazine, 16 (6), 6–10. doi: https://doi.org/10.1109/57.887599.

[6] Li, Y. (2019). Investigation of Heat Transfer Characteristics on Rod Fastening Rotor. IOP Conference Series: Materials Science and Engineering, 677 (3), 032032. doi: https://doi.org/10.1088/1757-899x/677/3/032032.

[7] Shibib, K., Minshid, M., Alattar, N. (2011). Thermal and stress analysis in Nd: YAG laser rod with different double end pumping methods. Thermal Science, 15, 399–407. doi: https://doi.org/10.2298/tsci101201004s.

[8] Andreev, V., Turusov, R. (2016). Nonlinear modeling of the kinetics of thermal stresses in polymer rods. Advanced Materials and Structural Engineering, 719–722. doi: https://doi.org/10.1201/b20958-150.

[9] Belytschko, T., Liu, W. K., Moran, B. (2000). Nonlinear Finite Elements for Continua and Structures. John Wiley and Sons.

[10] Wright, T. W. (2002). The Physics and Mathematics of Adiabatic Shear Bands. Cambridge University Press.

[11] Batra, R. C. (2006). Elements of Continuum Mechanics. AIAA. doi: https://doi.org/10.2514/4.861765.

[12] Sukarno, D. H. (2021). Analysis of nuclear fuel rod temperature distribution using CFD calculation and analytical solution. PROCEEDINGS OF THE 6TH INTERNATIONAL SYMPOSIUM ON CURRENT PROGRESS IN MATHEMATICS AND SCIENCES 2020 (ISCPMS 2020). doi: https://doi.org/10.1063/5.0058888.

[13] El-Azab, J. M., Kandel, H. M., Khedr, M. A., El-Ghandoor, H. M. (2014). Numerical Study of Transient Temperature Distribution in Passively Q-Switched Yb:YAG Solid-State Laser. Optics and Photonics Journal, 04 (03), 46–53. doi: https://doi.org/10.4236/ opj.2014.43007.

[14] Khany, S. E., Krishnan, K. N., Wahed, M. A. (2012). Study of Transient Temperature Distribution in a Friction Welding Process and its effects on its Joints. International Journal Of Computational Engineering Research, 2 (5), 1645.

[15] Mishchenko, A. (2020). Spatially Structure Spatial Problem of the Stressed-Deformed State of a Structural Inhomogeneous Rod. IOP Conference Series: Materials Science and Engineering, 953, 012004. doi: https://doi.org/10.1088/1757-899x/953/1/012004.

[16] Hwang, J.-K. (2020). Thermal Behavior of a Rod during Hot Shape Rolling and Its Comparison with a Plate during Flat Rolling. Processes, 8 (3), 327. doi: https://doi.org/10.3390/pr8030327.

[17] Logan, D. L. (2012). A First Course in the Finite Element Method. CENGAGE Learning, 727–764.

[18] Liu, Q., He, X. (2023). Thermal Analysis of Terfenol-D Rods with Different Structures. Micromachines, 14 (1), 216. doi: https:// doi.org/10.3390/mi14010216.

[19] Gaspar Jr., J. C. A., Moreira, M. L., Desampaio, P. A. B. (2011). Temperature Distribution on Fuel Rods: A study on the Effect of Eccentricity in the Position of UO2 Pellets. 20-th International Conference «Nuclear Energy for New Europe». Available at: https://arhiv.djs.si/proc/nene2011/pdf/814.pdf.

[20] Tashenova, Z., Nurlybaeva, E., Kudaykulov, A."Method preparation and solution algorithm for resolving stationary problem of a rod under thermo - stressed condition restrained at both ends affected by heat exchange and heat flows",Advanced Materials Research, vol. 875-877, pp.858–862, 2014, doi: 10.4028/www.scientific.net/AMR.875-877.858.

[21] Tashenova, Z.H.M., Nurlybaeva, E.N., Kudaikulov, A.K."Method of solution and computational algithm for mixed thermo-mechanics problem",World Applied Sciences Journal, vol. 28(12), pp. 2113–2119, 2013, doi: 10.5829/idosi.wasj.2013.28.12.422

[22] Tashenova, Z.M., Nurlybaeva, E.N., Kudaiykulov, A.K.Method of solution and computational algorithm for mixed thermo-mechanics problem",World Applied Sciences Journal, vol. 22(SPL.ISSUE2), pp. 49–57, 2013, doi: 10.5829/idosi.wasj.2013.22.tt.22139.

[23] Tashenova, Z.H.M., Zhumadillaeva, A.K., Nurlybaeva, E.N., Kudaykulov, A.K. "Numerical study of established thermo-mechanical state of rods of limited length, with the presence of local heat flows, temperatures, heat insulation and heat transfer",Advanced Science Letters, vol.19(8), pp. 2395–2397, 2013, doi: 10.1166/asl.2013.4926.

[24] K.K.Gornostaev,A.V.Kovalev,andY.V.Malygina, "Stress–strain state in an elastoplastic pipe taking into account the temperature and compressibility of the material," Journal of Physics: Conference Series,vol.973,2018.

[25] B. F. Shorr, "Termal integrity in mechanics and engineering," in Foundations of Termoelasticity, pp. 33–55, Springer, Berlin, Germany, 2015.

[26] O. C. Zienkiewicz and R. L. Taylor, Te Finite Element Method, Butterworth-Heinemann, Oxford, UK, 5th edition, 2000.